Polymer Bulletin
https://doi.org/10.1007/s00289-023-04827-0

ORIGINAL PAPER

Facile application of terahertz spectroscopy in UV-coated and phase change material loaded MPS

Emre Aytan[1,3] · Yusuf Samet Aytekin[2] · Tuğçe Akbal Aytan[1] · Okan Esenturk[2] · Memet Vezir Kahraman[1]

Received: 8 August 2022 / Revised: 21 November 2022 / Accepted: 5 May 2023

Abstract

In this study, capability of Terahertz (THz) spectroscopy for determination of thermal properties of phase change materials (PCM) in an acrylated polyurethane coating investigated. Spherical shaped mesoporous silica materials (MPSs) are prepared as a template for stearic acid (SA). SA was impregnated into MPSs for investigate its PCM properties. Surface of MPSs was modified with 3-(Trimethoxysilyl)propyl methacrylate (MEMO) to add acrylate functionality to form covalently bond to polyurethane (PU)-based composite UV matrix to avert leakage problem. Finally, this resin was photopolymerized and its change in thermal properties was determined by both conventional Differential Scanning Calorimetry (DSC) and THz. DSC results show that the heating process phase change enthalpy is measured between 20.83 J/g and 136.80 J/g, and the freezing process phase change enthalpy is found between 13.55 J/g and 181.13 J/g by DSC. The thermal properties of phase changing behavior of the sample were also analyzed by Terahertz Time Domain Spectroscopy (THz-TDS). Besides the phase changes THz spectroscopy has shown the temperature dependent variation in the host matrix, also final PCM sample. Comparison of the data suggest that THz Spectroscopy is a fairly strong technique for characterization of phase changing materials even in very complex resin environment and it is a strong complementary technique especially following the temperature dependent properties close to room temperature.

✉ Okan Esenturk
eokan@metu.edu.tr

✉ Memet Vezir Kahraman
mvezir@marmara.edu.tr

[1] Department of Chemistry, Marmara University, 34722 Istanbul, Turkey

[2] Department of Chemistry, Middle East Technical University, 06800 Ankara, Turkey

[3] Kimteks Poliüretan Sanayi Ve Ticaret A.Ş., Istanbul, Turkey

Published online: 20 May 2023

Graphical abstract

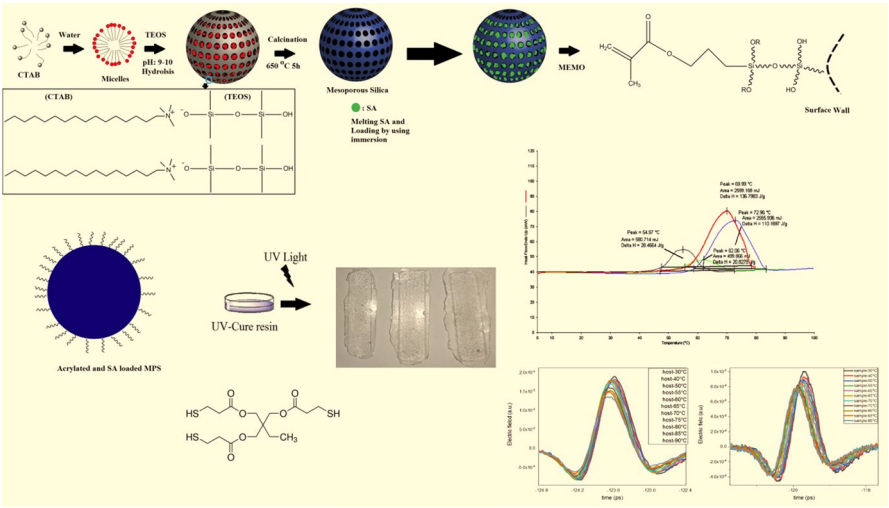

Keywords Mesoporous material · Differential scanning calorimetry (DSC) · Terahertz spectroscopy · Photopolymerization · Phase change materials

Introduction

Thermal energy storage methods have been introduced for large-scale applications to utilize thermal energy more efficiently. Phase change materials (PCMs) could be classed among these kind of thermal energy storage materials due to their high efficiency of storing and releasing large amount of latent heat during phase transitions [1–3]. PCMs are commonly classified as inorganic, organic and eutectic. Organic PCMs such as waxes, glycols, fatty alcohols, especially fatty acids, received more attention due to their superior properties such as being corrosive free, having better chemical stability, less supercooling and having better reversibility than their inorganic counterparts like metal alloys and salt hydrates. However, organic PCMs have some disadvantages like leakage, flammability and low thermal stability, which may hinder the usage of these materials [3–6].

Preparing various supporting structures for PCMs is one of the most common solutions to reduce or completely prevent the leakage of melted PCMs [7]. Organometallic frameworks (MOF), mesoporous silica, and mesoporous carbon materials have been developed as support matrices to achieve stabilized PCMs. Additionally, the disadvantages of PCMs could be reduced by preparing shape-stabilized PCM either by encapsulation method with inert coating shell or by integration into a porous structure [8, 9]. Lately, mesoporous silica nanomaterials (MSNs) gaining more attention to prepare porous matrices for obtaining ss-PCM. MSNs shows sufficient stability in term of chemical and thermal sense, good adsorption rate,

adjustable monodisperse pores in the 2–50 nm diameter range and their easy preparation methods allows their physicochemical properties to be easily adjustable. For example, Shen et al. doped lauric acid into modified sepiolite to prepare ss-PCM. Li et al. also developed stearic acid-based composite PCMs by using graphene-modified silica with vacuo impregnation technique to improve the thermal energy storage ability. In addition, Ince et al. [10–12] reported reduced extension of supercooling and thermal conductivity improvement by encapsulation of myristic acid with graphite nanoplates.

Enhancing the properties of MSN could be easily achieved by functionalization and modification of mesoporous silica (MPS) with organic and inorganic materials [13]. The addition of various functionalities proves to be useful to adjust both the surface chemistry and inner feature of the mesoporous materials. Octyl or octadecyl alkyl groups templated MPSs with both mesopores and macropores were synthesized and used as porous matrix for PCM consisting octadecanoic acid or octadecane. A maximum of 10.2 J/g heat of fusion value could be observed for the melting of the confined area. The confined heat of fusion observed higher for the longer functional group, due to stronger van der Waals forces between the functionalized silica surface and nano-confined phase change molecules [14].

Coating the PCMs in cross-linked structure is another method to prevent leakage problem of PCMs. In this method, PCM material is trapped in polymer matrix covalently or just physically. However, if the matrix is too dense it prevents the phase transition of PCMs. UV-curable coating method is used in various applications because of its cheap, energy saving, easy, and safe way to prepare supporting matrixes for PCMs [15]. Only requirements for this procedure are time, UV lamp and proper UV resin. Acrylic-based polyesters and polyurethanes are widely used in constructions, furniture, paints and alike industrial use [16].

As an emerging technology, Terahertz (THz) spectroscopy finds application in many fields on material characterization, especially the polymeric materials. THz range is generally considered as the frequency range of 0.1–20 THz, also referred as far-IR region of the electromagnetic spectrum. These frequencies have enough energy to couple with rotational, low frequency vibrational modes, and torsional modes of molecules [17]. Also the phonons, large scale lattice vibrations, are generally found in the THz regime, broadening the application possibility of THz spectroscopy for various purposes. On top of that THz waves with its relatively long wavelength are able to penetrate or pass through many materials like skin, paper, plastic, etc., bringing its potential use for in-line or on-line process analysis. With its unique properties THz spectroscopy technique has been utilized for many purposes like materials sciences [18], medicine and pharmaceutics [19, 20], as well as determination of explosive materials and weapons [21, 22]. THz-Time Domain Spectroscopy (THz-TDS) is a technique in which the transmitted THz pulse is measured in time domain. In this technique together with intensity, phase of the signal is also measured allowing complex-valued parameters to be extracted. Time domain nature of the THz-TDS also brings a new and quick way for routine analysis of the materials based on dielectric changes of the materials during certain processes such as phase changes. The PCMs are analyzed by various techniques, such as XRD, FTIR, SEM, TGA, and DSC. Being a new candidate, THz spectroscopy stands for a quite

promising technique with its genuine properties since THz waves are quite sensitive to different polymorphic forms of materials [23–26] and can readily be used for characterization of PCMs.

In this research, stearic acid material was impregnated in mesoporous silica and this mesoporous silica was coated by an acrylic resin. The change in enthalpy at every step was determined DSC method. Melting and freezing enthalpies are decreased every time that stearic acid was modified or impregnated into matrix and mesoporous silica. In addition, investigation of a new technique, THz-TDS, was performed to monitor temperature dependent behavior of the stearic acid in the matrix as a complementary way to monitor temperature dependent changes of phase changing materials.

Experimental

Materials

Tetraethyl orthosilicate(TEOS), NaOH, Cetyl trimethylammonium bromide(CTAB), stearic acid, 3-(Trimethoxysilyl)propyl methacrylate(MEMO), Daracure 1173™, Trimethylolpropane tris(3-mercaptopropionate) were all supplied from Sigma-Aldrich and Sartomer oligomer supplied from Arkema Group.

Synthesis of mesoporous silica

Mesoporous silica was synthesized by two step template removal method as in the literature [27] (Fig. 1). 1 g of CTAB was dissolved in water at 80 °C and then pH was increased to 10 by using 0,1 M NaOH into solution. CTAB takes the role of template and micelles were started to take form when TEOS is added into solution because of interaction between $-N^{+}$ of CTAB and $-O^{2-}$ in TEOS. The mixture was continuously stirred for 4 h at 80 °C and rested another 4 h without stirring for sedimentation which resulted in white solid silica particles. Solution was filtered and precipitate was dried at 100 °C for removal of trace amount water. Dried silica particles were calcinated at 650 °C for 5 h with a heating rate of 5 °C/min to remove of CTAB template. During calcinations progress the color first turned to orange and again turned to white. Final product was washed with ethanol and dried [28].

Impregnation of stearic acid and surface modification of MPS

Stearic acid was impregnated into MPSs by using evaporative impregnation, mesoporous silica and SA were put into ethanol ($60-750$ g L^{-1}), at 30 °C. The solvent was evaporated under vacuo at room temperature, and the remaining solids were collected and were used without any treatment.

Surface of MPS modified by using sol–gel method. [29] MEMO was hydrolyzed (3:1) in water at 50 °C. Meanwhile, SA loaded MPS were distributed in water in another pot. Hydrolyzed MEMO was added into MPS water mixture by dropwise

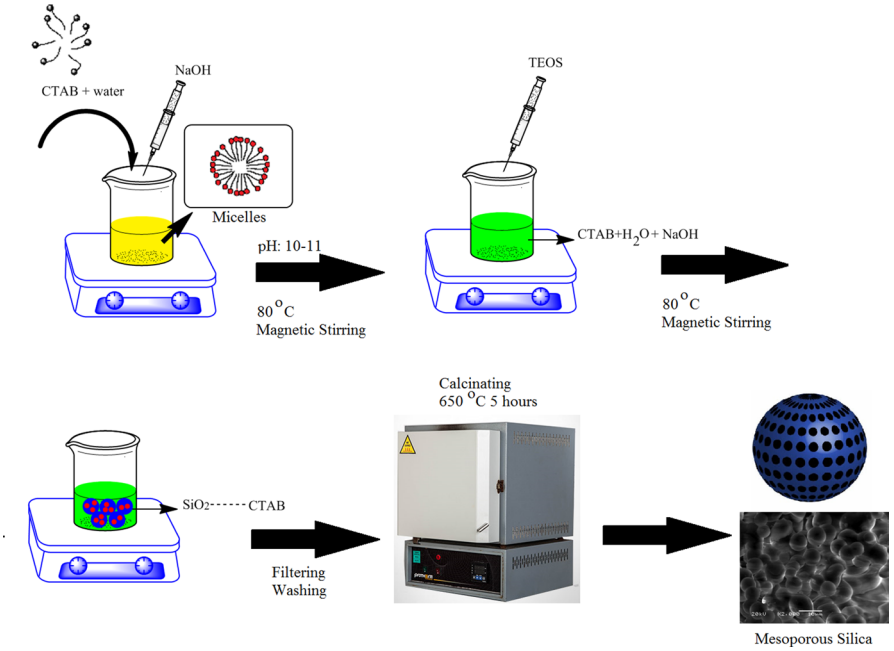

Fig. 1 Schematics of preparation of mesoporous silica

desired amount. Water was evaporated and washed with ethanol after addition of MEMO. Surface modification was observed by using FTIR. C=C bond appearance at 1633 cm^{-1} shows that modification was successful.

Preparation of UV-curable films

Commercially used acrylic-based polyurethane coating was prepared for our experiment. Coating resin was composed of oligomer, crosslinker, photoinitiator, antifoaming agent and modified MPSs. Aliphatic polyester-based urethane dimethacrylate oligomer Sartomer CN 1963 was used as oligomer, trifunctional Trimethylolpropane tris(3-mercaptopropionate) was used as crosslinker, Daracure 1173 as photoinitiator, BYK antifoaming agent A-1 as antifoaming agent and Modified MPS. The composition of membranes was 83%, 5%, 1% and 10%, respectively. To obtain uniform photo-cured films, they were put under a 300 W UV lamp and subjected to UV rays (OSRAM, λmax = 365 nm) for 3 min to induce polymerization.

Characterization

The chemical characterization of the samples was measured by ATR-FTIR spectroscopy. PerkinElmer Spectrum 100 ATR-FTIR spectrophotometer (PerkinElmer, Waltham, MA, USA) was used to record FTIR spectrum.

Philips L30 ESEM-FEG/ EDAX (Philips, Eindhoven, The Netherlands) was used for SEM measurements of samples. The samples were made ready for SEM analysis by freeze fracturing in liquid nitrogen following a gold coating.

Transmission electron microscopy (TEM) analysis was carried out in JEOL-JEM—1400 Plus. Size and morphology of samples were investigated by TEM analysis. Samples were dispersed in ethanol, dropped on 400 mesh CU grid and dried for TEM analysis.

The thermal stability of the films was determined in the temperatures between 30 and 750 °C by thermogravimetric analysis (TGA) using a PerkinElmer STA 6000 instrument (PerkinElmer, Waltham, MA, USA) under air atmosphere at a heating rate of 10 °C/min.

The PCM and thermal properties of samples were determined by using differential scanning calorimetry (DSC). The analysis was carried out with a Perkin Elmer Pyris Diamond model instrument (PerkinElmer, Shelton, CT, USA). The electrolytes were analyzed under a nitrogen atmosphere between of − 20 and 100 °C at a heating rate of 10 °C/min and cooling rate of 10 °C/min.

Phase changing properties of the samples were also monitored by the THz-TDS system. The details of the system have been described elsewhere [30]. In brief, an ultrafast mode locked Ti:Sapphire laser with pulse duration of 80 fs, central wavelength of 800 nm, and repetition rate of 80 MHz, was operated for THz generation and detection. An iPCA antenna is utilized for THz generation, while ZnTe crystal with < 100 > orientation was used for electro-optic sampling method as signal detection. The attained bandwidth range is 0.1–3.0 THz. The effective bandwidth changes with sample becomes up to ca. 1.5 THz. The measurements were done in a dry air purged environment (humidity less than ~ 1%) to minimize the attenuation caused by the water vapor. Fast Fourier transform with rectangular window function of the time domain data was applied to extract frequency domain data with a common software. [31] Measurements of the PCM samples were done between 30 °C and 90 °C with a temperature controlled sample holder. The temperature was raised gradually by 10 °C for temperatures lower than 50 °C and by 5 °C for the temperatures higher than 50 °C with a 5 min waiting at each temperature.

Results and discussion

Chemical characterization

All steps through synthesis to coating were observed by ATR-FTIR. Figure 2 shows the spectra of CTAB, CTAB template TEOS and TEOS. The sharp peak at

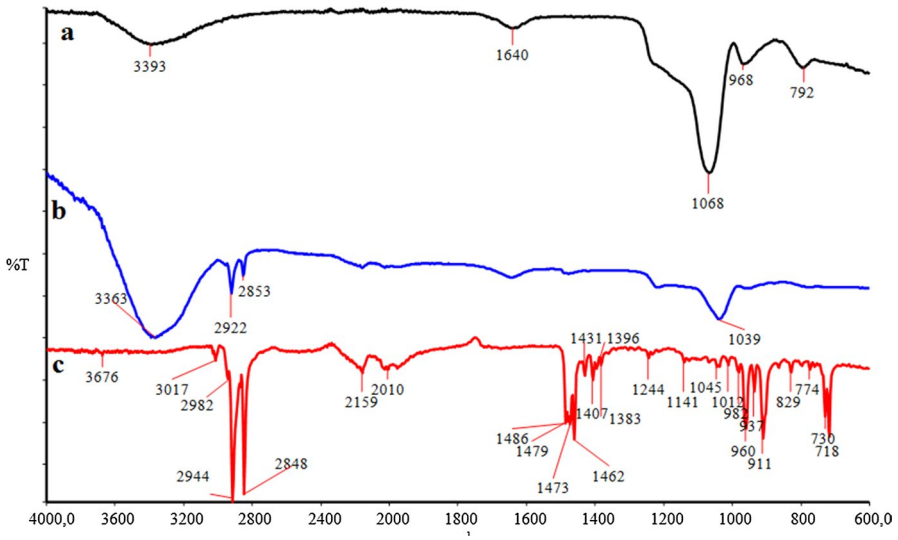

Fig. 2 FTIR spectra of bare TEOS (**a**), CTAB templated TEOS (**b**) and bare CTAB (**c**)

3017 cm^{-1} could be attributed to stretching of secondary amine(–N–H) group of CTAB (c) which could not observed when it was reacted with TEOS (a) to form template of spherical structure with TEOS (b). Hence it indicates the interaction between SiO_2 groups on TEOS and quaternary amine (-N^+H3Br^-) of CTAB. Three sharp peaks at 2982 cm^{-1}, 2944 cm^{-1} and 2848 cm^{-1} in the spectra of CTAB(ca) could be attributed to stretching of secondary amine group in addition to stretching and anti-stretching of C–H, respectively. However, when spectra of CTAB template TEOS (b) investigated, the characteristic peaks of these secondary amine and alkyl groups appear to be either weakened or shifted. In the spectra of CTAB spectra (c), sharp peaks were observed between 1380 cm^{-1} and 1490 cm^{-1} and these peaks could be attributed to asymmetrical and symmetrical C-H scissoring vibration of H_3C–N moiety, also two strong peaks at 1462 cm^{-1} and 960 cm^{-1} could be attributed to stretching of C–N, the peak at 1141 cm^{-1} could be attributed to –N–H bending and peak at 1640 cm^{-1} of both mesoporous materials represented the bending vibration of hydroxyl groups [32–34].

Figure 3 shows the spectra of calcinated MPSs (a), bare SA (b) and SA loaded MPSs(c). All the organic groups related peaks were disappeared due to calcinations due to calcinations process. Only strong and wide –OH stretching peaks at 3395 cm^{-1} of silanol groups condensation is present. The characteristic peaks of symmetrical and asymmetrical stretching of Si–O-Si groups were observed between 1067 cm^{-1} and 792 cm^{-1}. The results showed that condensation of Si–OR groups and extraction of CTAB template were achieved [35]. In the spectrum of bare SA, the bands at 1461 and 1428 cm^{-1} is caused by the bending vibration of the functional group $-CH_2-COOH$. Sharp peaks at 2909 and 2847 cm^{-1} can be attributed to the asymmetrical and symmetrical vibration of the $-CH_2$ group, respectively. In addition, peaks at 718 cm^{-1}, 687 cm^{-1} and 932 cm^{-1} could be attributed to in-plane

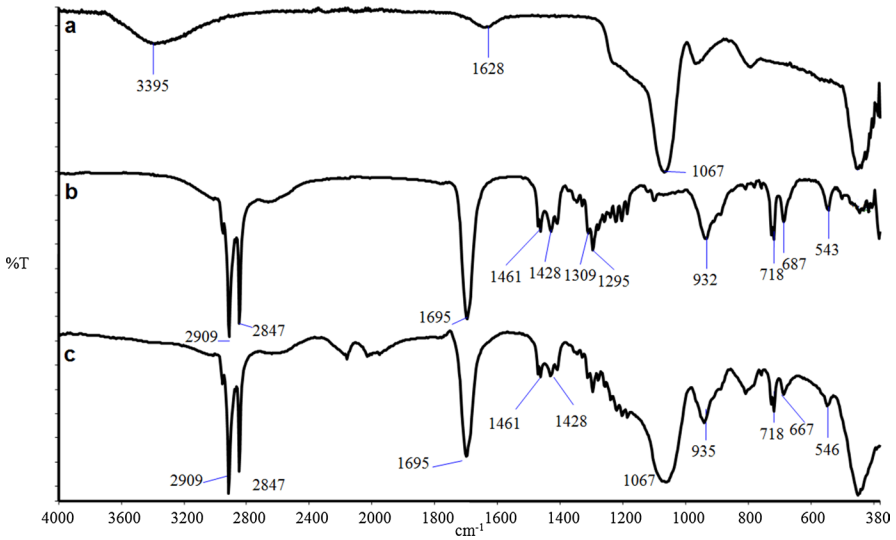

Fig. 3 FTIR spectra of calcinated MPSs (**a**), bare SA (**b**) and SA loaded MPSs (**c**)

swinging and out-of-plane bending vibrations of the hydroxyl (-OH) group, respectively [36]. One can see that every characteristic peaks that discussed above are present after impregnation of SA into MPSs. Shifting and peak intensity changes can be attributed to van der Waals interaction and H bonding between functional groups of MPSs and SA [37, 38].

Figure 4 shows the spectra of surface modification of SA loaded MPSs with MEMO (a), photo-curable Resin (b), and photo-cured films (c). The characteristic peak of C=C bond appeared at 1633 cm^{-1} and this indicates that surface modification of SA loaded MPSs were success. Sharp peak at 1709 cm^{-1} can be attributed to urethane bond and peaks at 1636 cm^{-1} and 1616 cm^{-1} could be attributed to C=C bonds on photo-curable resin [39]. After photo polymerization process all the C=C peaks disappeared which means the polymerization was success.

Thermal characterization

TGA and DSC methods are conventional methods for determining thermal properties. The change in phase change properties SA were examined step by step by DSC method. Bare SA (a) shows melting behavior between from 52 to 78 °C with a peak of 69.99 °C. The enthalpy (ΔH) value of this melting determined as 136.8 J/g. However, this value decreased each time when it is covered by a layer. In the DSC thermogram SA loaded MPSs shows melting behavior but it is obvious that this melting behavior result of SA which is confined in silica spheres [40]. The shift in melting temperature can be attributed to release hindering due to van der Waals interactions between SA and MPSs [41]. ΔH value lowered to 110.17 J/g. The enthalpy value even more lowered after surface modification of MPSs with MEMO which casted another layer and hindered enthalpy to

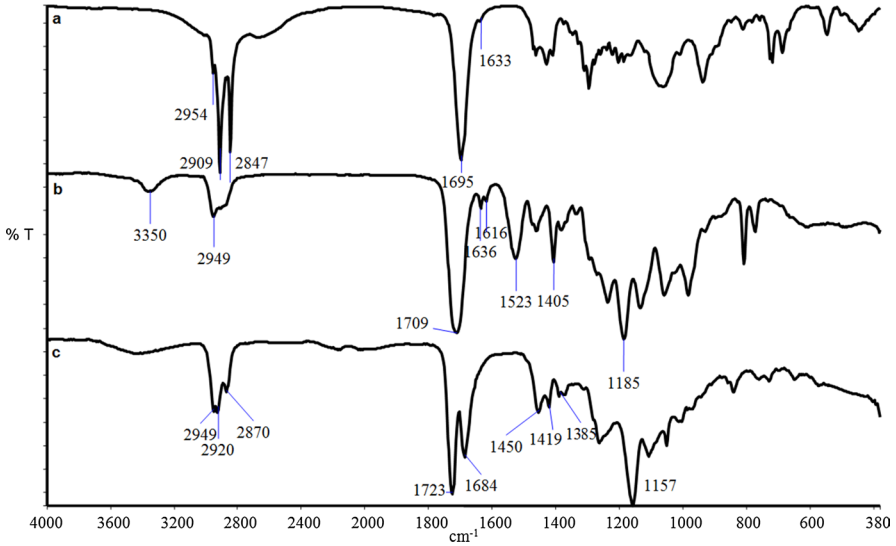

Fig. 4 FTIR spectra of SA loaded MPSs with MEMO (**a**), photo-curable Resin (**b**), and photo-cured films (**c**)

28.47 J/g. Finally, the sample was coated with acrylic-based polyurethane resin which is a highly crosslinked structure and resulted in lowering of ΔH value. However, sample showed 20.83 J/g ΔH value. The freezing behaviors of samples are similar to melting behavior. Freezing enthalpies of bare SA, SA loaded MPSs, MEMO modified MPSs and coated samples are 181.14 J/g, 171.52 J/g, 41.36 J/g and 13.56 J/g. However one can say that coated samples were more protected against heating and cooling due to highly cross linked structure.

Thermal stability is one of the important parameters of thermal energy storage applications therefore stability of samples was determined by TGA. TGA spectrum of samples was presented in Figs. 5 and 6. SA impregnated MPSs shows a characteristic organic compound decomposition behavior. Sharp weight loss began at 200 °C and ended at 270 °C. Remaining 9% ash shows that MPSs could be loaded more than ten times than their weight. MEMO modified sample and PCM containing PU film underwent chemical dehydration process between 200 °C and 400 °C which resulted in 9% water evaporation [42]. Over 400 °C, MEMO and carbon backbone of PU samples started to decompose Fig. 7. Blank polyurethane film sample started to decompose at 320 °C. TGA results are given in Table 1.

Addition of inorganic material into polymer matrix which hinders the crystalline packing during photopolymerization process leads to improving physical properties of polymers. However, it also causes less inter-chain interactions in polymer matrix. Thus; it could be attributed that shifting in onset value of PU films could be explained by integration of inorganic MPSs and MEMO into polymer matrix. As a result, more flexible chains produced during photopolymerization and decomposition temperature decreased due to less chain interactions. Additionally, char yield

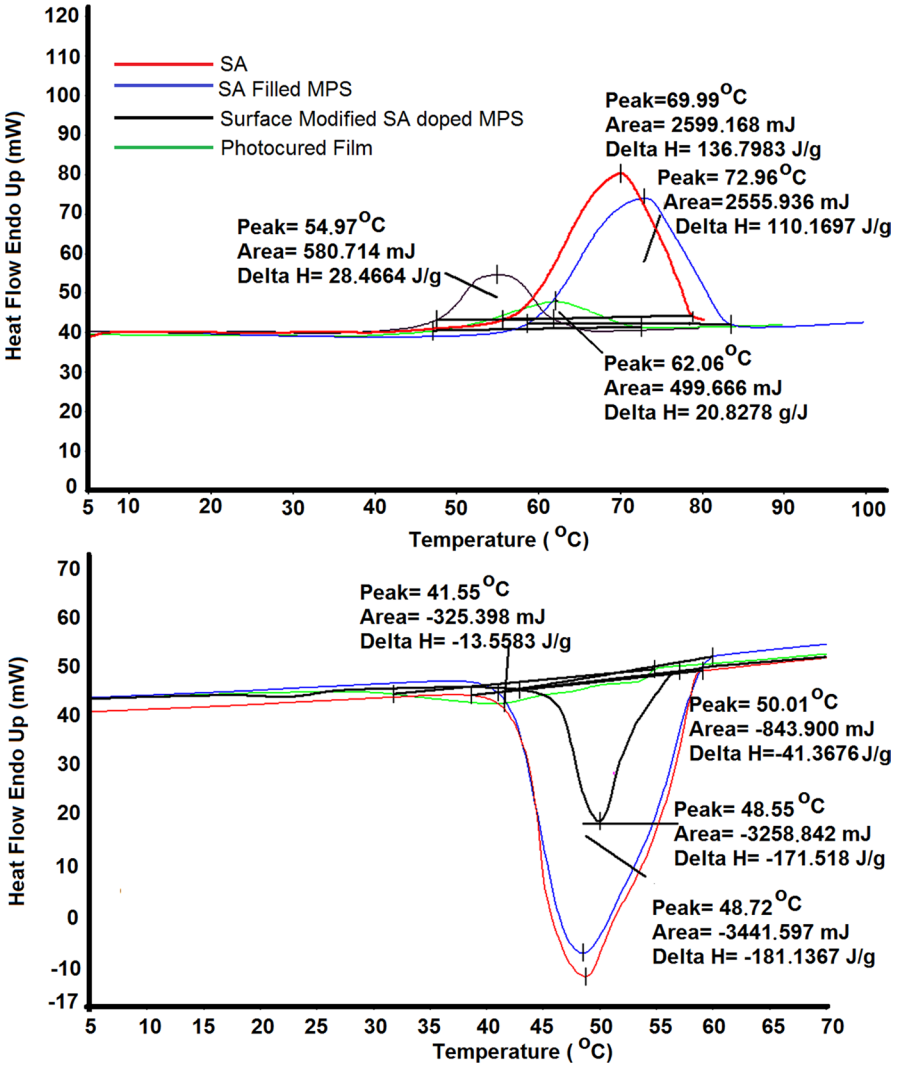

Fig. 5 DSC Thermogram of samples

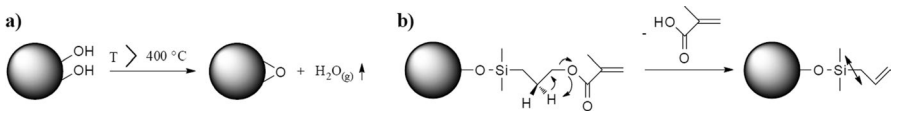

Fig. 6 **a** Chemical dehydration process **b** Methacrylic acid loss by McLafferty rearrangement in the thermal degradation of MEMO [42]

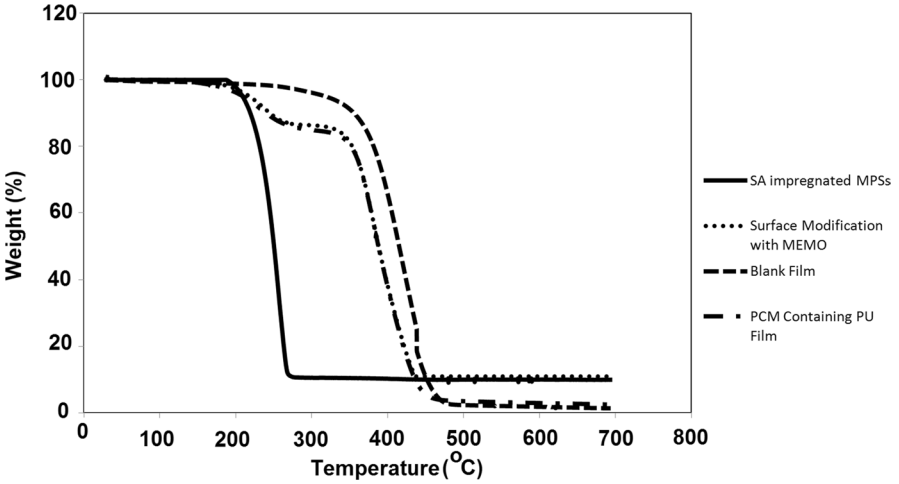

Fig. 7 TGA Thermogram of samples

Table 1 TGA results of samples

Sample	$T_{\%10}$	T_{onset}	Ash weight %
SA impregnated MPSs	219.22	250.26	9.896
Surface modification with MEMO	245.26	388.22	11.07
Blank PU film	355.58	415.12	1.306
PCM containing PU film	239.4	388.51	2.469

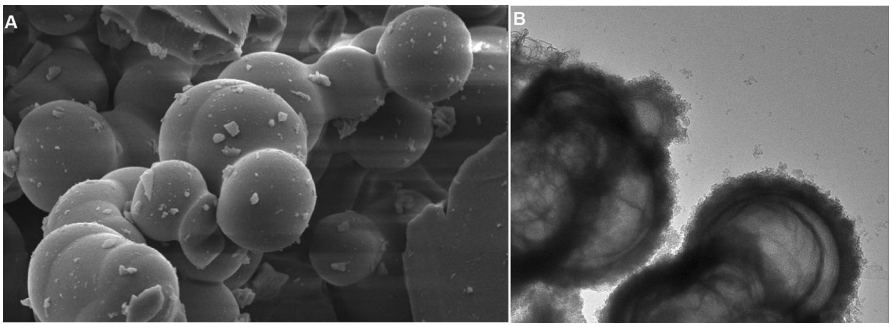

Fig. 8 SEM (**A**) 0 and TEM (**B**) Images of MPSs

was examined and it was found that amount of char yield was increased due to additional inorganic MPS material [43].

Morphology

Geometrical shape of product by sol–gel method depends on some factors. Two of them are interaction between template and silyl groups and pH value. When the pH value is alkali with template, it is possible to produce rod-like and spherical materials [44]. Morphology of the obtained materials was analyzed with SEM and TEM and images are shown in Fig. 8. In SEM image (8-A), spherical materials were produced successfully after removal of template by calcinations. Moreover, TEM image (8B) showed that there are worm-like channels formed by the removal of template.

Terahertz spectroscopy

The temperature dependent behavior of the samples (blank PU film and PCM containing PU film) was also analyzed with THz-TDS technique. Time domain profile and corresponding frequency domain spectra at room temperature of the host and the sample as representative spectra are given in Fig. 9. While both samples exhibited slight changes in the profiles of both time domain and corresponding frequency domain spectra, clear differences can be realized between the host and PCM containing sample curves in both domains due to differences in their dielectric medium. The PCM introduces extra delay in time domain due to index change (Fig. 9a) and extra loss in the THz amplitude (Fig. 9b).

The temperature dependent changes in the time domain profiles and the corresponding frequency domain spectra of the host and impregnated sample are shown in Fig. 10. The THz time domain profile is highly sensitive to the dielectric behavior of the materials. If there is any change in materials absorbance or index behavior in THz region, it will result in changes in THz profile of the sample. It may result in attenuation or shift in the position. This enables to sensitively follow the behavior of the material under changing conditions such as temperature. In the host and the sample, both the peak position of the THz profile is shifted in time and the THz amplitude has decreased due to the changes in both host's and sample's properties

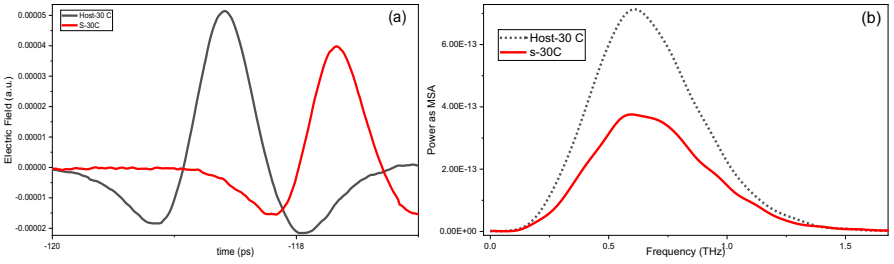

Fig. 9 Room temperature **a** time domain profile of the host and sample, and **b** corresponding frequency domain spectra of them

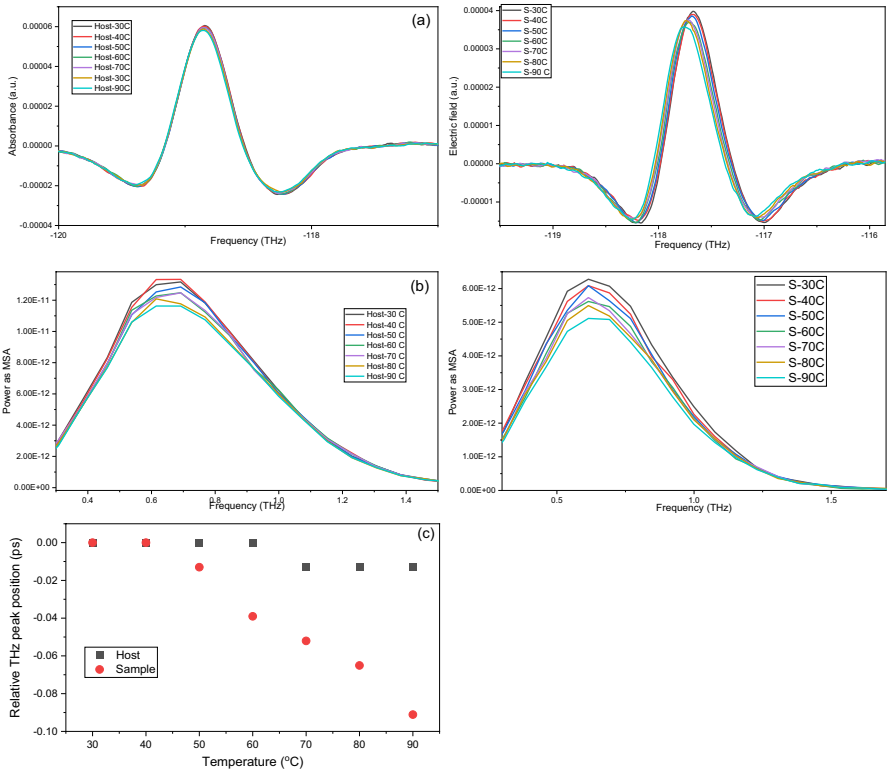

Fig. 10 Temperature dependent **a** time domain profile of the host and the sample, **b** corresponding frequency domain spectra of them, and **c** relative peak position of the host and the sample as the temperature changes

as the temperature was increased. The attenuation usually mainly owes to changes in absorption characteristics of the materials, while the shift in time is due to changes in the refractive index of the materials, assuming index change is low with the temperature increase. THz wave attenuation (the decrease in this case) has been observed for both the host and the sample in the time domain profiles. This results in an amplitude decrease in the corresponding frequency domain spectra where both the host and the sample have featureless and broad spectra. (Fig. 10b) Though the observed attenuation behaviors of the host and sample films looks similar, amplitude of the sample changes slightly more with the temperature than the host material. For example, at 0.61 THz (at the maximum amplitude point) the change in THz amplitude between the 30 °C and 90 °C is about 19% for the sample while it is about 13% for the host.

Changes in the THz time domain profile of the host or the sample with temperature does also provide information about the dielectric behaviors with temperature. A positive change (right shift) is suggesting an increase in refractive index on the other hand, a negative change (left shift) refers to a decrease in the index.

Interestingly, both the host and the sample showed a negative change in these measurements. However, the amounts of the change were significantly different in both measurements. Figure 10a shows that the blank film (host) has a left shift as the temperature is increased from 30 to 90 with a total change of 1.3×10^{-2} ps. On the other hand, the total shift in the PCM containing PU film is around 7.8×10^{-2} ps within the same temperature range. Figure 10c shows the peak position tracking of the host and the sample THz beam profiles. Even though the sample thickness is around the twice the thickness of the reference host ($d_{\text{sample}} = 1.186$ mm; $d_{\text{host}} = 0.578$ mm), the observed left shift in the time domain is three times more (thickness corrected) than the shift observed in the reference sample between 30 and 90 °C profiles. One of the possibilities in the observed left shift of the materials could be due to the thermal expansion of the host. However, then shift amount should have been correlated with the thickness of the sample, which is not, as shown. In addition, we have checked the films thickness for both host and the sample films and did not observe any thickness change after both films being kept in the 65 °C oven for 30 min. Therefore, the main difference must be associated with the introduction of the PCM material into the host and its phase changing capabilities. In fact, a closer look into the data shows that the difference between the host and the sample starts with the phase changing behavior of the SA. In order to show the differences clearly, shifts in peak positions of the host (full black squares) and the PCM containing film (full red circles) in time domain spectra are given in Fig. 10c. Here we noticed that up to 70 °C there is almost no change in the peak position of the host material. After 70 °C, we have noticed that the peak position is very slightly shifted with temperature but then stayed almost the same. This might be associated with the SNR rather than a real change in the peak position. Since no phase change is expected in this sample, these changes are attributed to a very slight changes in the dielectric property of the host with temperature, showing THz-TDS's high sensitivity on observation of changes in dielectric behavior of the material. On the other hand, the sample peak position does change significantly with temperature. In fact, it closely follows the DSC thermogram (Fig. 5a, green line). A significant change starts after 40 °C up to 60 °C, and later behavior follows the trend. We have also investigated the THz amplitude changes with the temperature in frequency domain and observed roughly the similar transmission changes with temperature when corrected with respect to the thicknesses of the host and sample.

Figure 10c showed the peak position tracking of the host and the sample, which approximately corresponds to the average index change of the measured material. In Fig. 11a and b, the frequency dependent refractive indices of the both the host and the sample is given, respectively. Figure 11c is showing the refractive index change of the both at ca. 0.6 THz. Up to 40 °C there are similar slight changes for the host and sample films. After 40 °C the host did not change much and a similar behavior is observed up to 80 °C, similar to the peak position behavior in time domain. Comparison of the host and the sample behavior suggest that the phase changing behavior of the sample starts after 40 °C and continues up to 80 °C with less steep change between 60 and 80 °C. Interestingly enough that the sample also shows a slight increase at 90 °C as its host material, possibly due to an anomaly behavior of the host. Overall the index behavior is very similar to the DSC thermogram of the

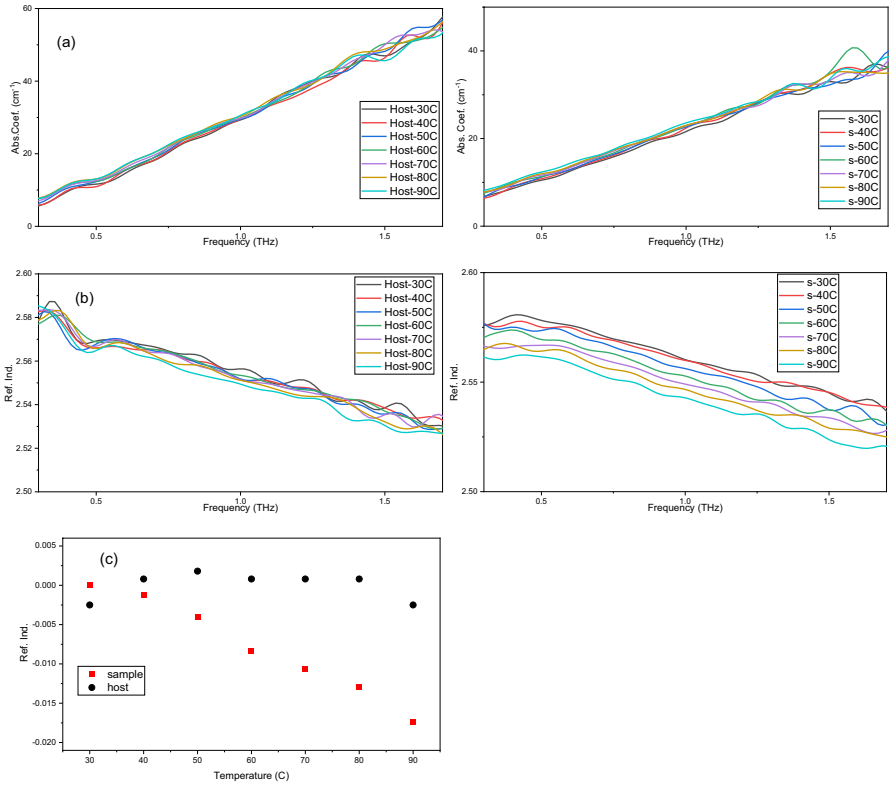

Fig. 11 **a** Absorption coefficient spectra, **b** Refractive Index of the host and the sample films, and **c** refractive index change with temperature of the host and the sample at 0.6 THz

sample. The results show the strong ability of the THz-TDS and its complementary nature on thermal characterization of the phase changing materials even in a host matrix.

Conclusion

MEMO modified and SA containing MPSs were prepared and integrated into photo-curable coating. Photo crosslinked PCM material were formed by UV polymerization to prevent leakage problem according to the literature. TGA results shows that prepared PCMs containing films stable under 300 °C, which is much superior than bare fatty acids and alcohols. Thermal phase change properties of PCMs are investigated by DSC and results indicates that every additional layer on SA lowers its enthalpy (1368 to 2083 J/g) value. In addition to conventional PCM property determination technique, THz spectroscopy was also applied to determine phase changing properties of photo-cured PCMs in this research. Results of both DSC and THz techniques show consistency and a detailed and sensitive phase changing

information appears to be obtained by THz-TDS technique. THz spectroscopy is an emerging as a novel technique in order to characterize of PCM and could be take into account as a complementary technique to the traditional thermal phase transition analysis techniques.

Acknowledgements This work was supported by Marmara University, Commission of Scientific Research Project (M.U.BAPKO) under grant FEN-C-DRP-200318-0118

Author contributions Authors contributed this manuscript as follows; EA contributed to conceptualization, methodology, validation, formal analysis, investigation, resources, data curation, writing–original draft, writing–review and editing, and visualization. SA contributed to conceptualization, methodology, validation, formal analysis, investigation, resources, data curation, writing–original draft, writing–review and editing, software, and visualization. TAA contributed to conceptualization, methodology, validation, formal analysis, investigation, resources, data curation, writing–original draft, writing–review and editing. OE contributed to conceptualization, methodology, validation, formal analysis, investigation, resources, data curation, writing–original draft, writing–review and editing, software, supervision, and project administration. MVK contributed to conceptualization, methodology, validation, formal analysis, investigation, resources, data curation, writing–original draft, writing–review and editing, software, supervision, and project administration.

Declarations

Conflict of interest The authors declare that they have no known competing financial interests or personal relationships that could have appeared to influence the work reported in this paper.

Ethical approval Authors declares that manuscript was prepared according to ethic code of the journal and "No human or animal experiment" involved in research.

Consent for publication All authors gave their consent for the submission of this article.

References

1. Huang X, Alva G, Jia YT et al (2017) Morphological characterization and applications of phase change materials in thermal energy storage: a review. Renew Sustain Energy Rev 72:128–145
2. Oró E, de Gracia A, Castell A, Farid MM, Cabeza LF (2012) Review on phase change materials (PCMs) for cold thermal energy storage applications. Appl Energy 99:513–533
3. Baetens R, Jelle BP, Gustavsen A (2010) Phase change materials for building applications: a state-of-the-art review. Energy Build 42:1361–1368
4. Sharma A, Tyagi VV, Chen CR, Buddhi D (2009) Review on thermal energy storage with phase change materials and applications. Renew Sustain Energy Rev 13:318–345
5. Wang Z et al (2014) Rapid charging of thermal energy storage materials through plasmonic heating. Sci Rep 5:6246
6. Chen F, Wolcott MP (2014) Miscibility studies of paraffin/polyethylene blends as form-stable phase change materials. Eur Polym J 52:44–52
7. Zhang XG, Liu HT, Huang ZH, Yin ZY, Wen RL, Min X, Huang YT, Fang MH, Liu YG, Wu XW (2016) Preparation and characterization of the properties of polyethylene glycol@ Si3N4 nanowires as phase-change materials. Chem Eng J 301:229–237
8. Su WG, Darkwa J, Kokogiannakis G (2015) Review of solid−liquid phase change materials and their encapsulation technologies. Renew Sustain Energy Rev 48:373–391
9. Qian TT, Li JH, Ma HW, Yang J (2015) The preparation of a green shape-stabilized composite phase change material of polyethylene glycol/SiO2 with enhanced thermal performance based on oil shale ash via temperature-assisted sol-gel method. Sol Energy Mater Sol Cells 132:29–39

10. Shen Q, Ouyang J, Zhang Y, Yang H (2017) Lauric acid/modified sepiolite composite as a form-stable phase change material for thermal energy storage. Appl Clay Sci 146:14–22. https://doi.org/10.1016/j.clay.2017.05.035
11. Li B, Liu T, Hu L, Wang Y, Nie S (2013) Facile preparation and adjustable thermal property of stearic acid−graphene oxide composite as shape-stabilized phase change material. Chem Eng J 215–216:819–826
12. İnce Ş, Seki Y, Akif Ezan M, Turgut A, Erek A (2015) Thermal properties of myristic acid/graphite nanoplates composite phase change materials. Renew Energy 75:243–248. https://doi.org/10.1016/j.renene.2014.09.053
13. Trewyn BG, Slowing II, Giri S, Chen H-T, Lin VS-Y (2007) Synthesis and functionalization of a mesoporous silica nanoparticle based on the sol-gel process and applications in controlled release. Acc Chem Res 40(9):846–853. https://doi.org/10.1021/ar600032u
14. Wang Y, Zhang L, Tao S, An Y, Meng C, Hu T (2014) Phase change in modified hierarchically porous monolith: an extra energy increase. Microporous Mesoporous Mater 193:69–76. https://doi.org/10.1016/j.micromeso.2014.03.007
15. Baştürk E, Kahraman MV (2016) Photocrosslinked biobased phase change material for thermal energy storage. J Appl Polym Sci. https://doi.org/10.1002/app.43757
16. Baştürk E, Kahraman MV (2018) Preparation and performances of UV-cured methacrylated polyacrylic acid-based core-shell hybrid phase change materials. Polym Eng Sci. https://doi.org/10.1002/pen.24829
17. Baxter JB, Guglietta GW (2017) Terahertz spectroscopy, vol 83. CRC Press, Boca Raton
18. Spies JA et al (2020) Terahertz spectroscopy of emerging materials. J Phys Chem C 124(41):22335–22346. https://doi.org/10.1021/acs.jpcc.0c06344
19. Zeitler JA, Taday PF, Newnham DA, Pepper M, Gordon KC, Rades T (2010) Terahertz pulsed spectroscopy and imaging in the pharmaceutical setting–a review. J Pharm Pharmacol 59(2):209–223. https://doi.org/10.1211/jpp.59.2.0008
20. Parrott EPJ, Sun Y, Pickwell-MacPherson E (2011) Terahertz spectroscopy: its future role in medical diagnoses. J Mol Struct 1006(1–3):66–76. https://doi.org/10.1016/j.molstruc.2011.05.048
21. Federici JF et al (2005) THz imaging and sensing for security applications—explosives, weapons and drugs. Semicond Sci Technol 20(7):S266–S280. https://doi.org/10.1088/0268-1242/20/7/018
22. Davies AG, Burnett AD, Fan W, Linfield EH, Cunningham JE (2008) Terahertz spectroscopy of explosives and drugs. Mater Today 11(3):18–26. https://doi.org/10.1016/S1369-7021(08)70016-6
23. Lu C, Lu Q, Gao M, Lin Y (2021) Dynamic manipulation of THz waves enabled by phase-transition VO2 thin film. Nanomaterials 11(1):114. https://doi.org/10.3390/nano11010114
24. Sibik J, Sargent MJ, Franklin M, Zeitler JA (2014) Crystallization and phase changes in paracetamol from the amorphous solid to the liquid phase. Mol Pharm 11(4):1326–1334. https://doi.org/10.1021/mp400768m
25. Calvo NL, Maggio RM, Kaufman TS (2018) Chemometrics-assisted solid-state characterization of pharmaceutically relevant materials. Polymorphic substances. J Pharm Biomed Anal 147:518–537. https://doi.org/10.1016/j.jpba.2017.06.018
26. Rexrode NR, Orien J, King MD (2019) Effects of solvent stabilization on pharmaceutical crystallization: investigating conformational polymorphism of probucol using combined solid-state density functional theory, molecular dynamics, and terahertz spectroscopy. J Phys Chem A 123(32):6937–6947. https://doi.org/10.1021/acs.jpca.9b00792
27. Wu S-H, Mou C-Y, Lin H-P (2013) Synthesis of mesoporous silica nanoparticles. Chem Soc Rev 42(9):3862. https://doi.org/10.1039/c3cs35405a
28. Wei T, Zheng B, Liu J, Gao YF, Guo WH (2014) Structures and thermal properties of fatty acid/expanded perlite composites as form-stable phase change materials. Energy Build 68:587–592
29. Çok SS, Koç F, Gizli N (2020) Hydrophobic silica aerogels synthesized in ambient conditions by preserving the pore structure via two-step silylation. Ceram Int. https://doi.org/10.1016/j.ceramint.2020.07.278
30. Aytekin YS, Köktürk M, Zaczek A, Korter TM, Heilweil EJ, Esenturk O (2018) Optical properties of meloxicam in the far-infrared spectral region. Chem Phys 512:36–43. https://doi.org/10.1016/j.chemphys.2018.04.022
31. Hoshina H (2011) TDS spectrum viewer. Tokyo, [Online]. Available: http://www.riken.jp/lab-www/THz-img/hoshina/software_e.html
32. Ramos Guivar JA, Sanches EA, Magon CJ, Ramos Fernandes EG (2015) Preparation and characterization of cetyltrimethylammonium bromide (CTAB)-stabilized Fe 3 O 4 nanoparticles for

electrochemistry detection of citric acid. J Electroanal Chem 755:158–166. https://doi.org/10.1016/j.jelechem.2015.07.036
33. Nithiyanantham U, Ede SR, Ozaydin MF, Liang H, Rathishkumar A, Kundu S (2015) Low temperature, shape-selective formation of Sb 2 Te 3 nanomaterials and their thermoelectric applications. RSC Adv 5(109):89621–89634
34. Criado M, Sobrados I, Sanz J (2014) Polymerization of hybrid organic–inorganic materials from several silicon compounds followed by TGA/DTA, FTIR and NMR techniques. Prog Org Coat 77(4):880–891. https://doi.org/10.1016/j.porgcoat.2014.01.019
35. Al-Oweini R, El-Rassy H (2009) Synthesis and characterization by FTIR spectroscopy of silica aerogels prepared using several Si(OR)4 and R″Si(OR′)3 precursors. J Mol Struct 919(1–3):140–145. https://doi.org/10.1016/j.molstruc.2008.08.025
36. Huang H, Tian M, Yang J, Li H, Liang W, Zhang L, Li X (2007) Stearic acid surface modifying Mg(OH)2: mechanism and its effect on properties of ethylene vinyl acetate/Mg(OH)2 composites. J Appl Polym Sci 107(5):3325–3331. https://doi.org/10.1002/app.24894
37. Wei H, Xie X, Li X, Lin X (2016) Preparation and characterization of capric-myristic-stearic acid eutectic mixture/modified expanded vermiculite composite as a form-stable phase change material. Appl Energy 178:616–623. https://doi.org/10.1016/j.apenergy.2016.06.109
38. Yi H, Zhan W, Zhao Y, Qu S, Wang W, Chen P, Song S (2019) A novel core-shell structural montmorillonite nanosheets/stearic acid composite PCM for great promotion of thermal energy storage properties. Sol Energy Mater Sol Cells 192:57–64. https://doi.org/10.1016/j.solmat.2018.12.015
39. Wu KC, Halloran JW (2005) Photopolymerization monitoring of ceramic stereolithography resins by FTIR methods. J Mater Sci 40(1):71–76. https://doi.org/10.1007/s10853-005-5689-y
40. Chen Y, Zhang X, Wang B, Lv M, Zhu Y, Gao J (2017) Fabrication and characterization of novel shape-stabilized stearic acid composite phase change materials with tannic-acid-templated mesoporous silica nanoparticles for thermal energy storage. RSC Adv 7(26):15625–15631. https://doi.org/10.1039/c7ra00964j
41. Matei C, Buhălţeanu L, Berger D, Mitran R-A (2019) Functionalized mesoporous silica as matrix for shape-stabilized phase change materials. Int J Heat Mass Transf 144:118699. https://doi.org/10.1016/j.ijheatmasstransfer.2019.118699
42. Cappelletti AL, Paez JI, Strumia MC (2011) Synthesis and characterization of thermo-sensitive magnetic maghemite nanoparticles. ARKIVOC. https://doi.org/10.3998/ark.5550190.0012.735
43. Aytan E, Uğur MH, Kayaman-Apohan N (2019) Synthesis, characterization, and ionic conductivity of electrospun organic–inorganic hybrid gel electrolytes. Polym Eng Sci. https://doi.org/10.1002/pen.25320
44. Li X, Shi B, Chaikittisilp W, Li M, Wang Y, Liu Y, Mao L (2016) A general method to synthesize a family of mesoporous silica nanoparticles less than 100 nm and their applications in anti-reflective/fogging coating. J Mater Sci 51(13):6192–6206. https://doi.org/10.1007/s10853-016-9916-5